Molecular Lanthanide Switches for Magnetism and Photoluminescence

Luca Münzfeld, Milena Dahlen, Adrian Hauser, Nolwenn Mahieu, Senthil Kumar Kuppusamy, Jules Moutet, Maxime Tricoire, Ralf Köppe, Léo La Droitte, Olivier Cador, et al.

How to cite: *Angew. Chem. Int. Ed.* **2023,** *62,* e202218107
International Edition: doi.org/10.1002/anie.202218107
German Edition: doi.org/10.1002/ange.202218107

Molecular Switches

Molecular Lanthanide Switches for Magnetism and Photoluminescence

Luca Münzfeld, Milena Dahlen, Adrian Hauser, Nolwenn Mahieu, Senthil Kumar Kuppusamy, Jules Moutet, Maxime Tricoire, Ralf Köppe, Léo La Droitte, Olivier Cador, Boris Le Guennic, Grégory Nocton, Eufemio Moreno-Pineda, Mario Ruben,* and Peter W. Roesky**

Abstract: Solvation of [(CNT)Ln(η^8-COT)] (Ln = La, Ce, Nd, Tb, Er; CNT = cyclononatetraenyl, i.e., $C_9H_9^-$; COT = cyclooctatetraendiid, i.e., $C_8H_8^{2-}$) complexes with tetrahydrofuran (THF) gives rise to neutral [(η^4-CNT)Ln(thf)$_2$(η^8-COT)] (Ln = La, Ce) and ionic [Ln(thf)$_x$(η^8-COT)][CNT] (x = 4 (Ce, Nd, Tb), 3 (Er)) species in a solid-to-solid transformation. Due to the severe distortion of the ligand sphere upon solvation, these species act as switchable luminophores and single-molecule magnets. The desolvation of the coordinated solvents can be triggered by applying a dynamic vacuum, as well as a temperature gradient stimulus. Raman spectroscopic investigations revealed fast and fully reversible solvation and desolvation processes. Moreover, we also show that a Nd:YAG laser can induce the necessary temperature gradient for a self-sufficient switching process of the Ce(III) analogue in a spatially resolved manner.

Introduction

In recent years, the intriguing physical properties of lanthanide compounds and materials, that originate from their partially filled 4f-orbitals resulted in a surge of novel synthetic methods and theoretical approaches. Research has mainly been focused on the development of single-molecule magnets (SMMs) and luminescent compounds.[1] Both are often aiming at future applications in advanced technological devices. These promising prospects in particular stimulated the search for high-performance SMMs that could practically be integrated in real-world data storage architectures and quantum computers.[2] Most systems developed in this context rely on rigid and strongly bonded ligand moieties that can be specifically tailored to enhance the anisotropic properties of lanthanide ions.[3] However, this often contradicts another field of possible applications that has attracted considerable attention; that of molecular (quantum) sensors and switches, which are envisioned to play an important future role in the design and construction of functional devices at the molecular level.[4] To fulfil this purpose, the target compounds' electronic structure should be manipulatable by a low energetic external stimulus, such as thermal,[5] mechanical,[6] redox,[7] photo,[8] and solvation[9] processes.

The aim of this work was to find a simple and flexible platform providing tools for the facile reversible manipulation of magnetic and photophysical properties in trivalent lanthanide organometallic compounds. We decided to tackle this task by combining findings from our groups, involving the CNT anion.[10] Specifically, the smooth transfer of synthetic protocols developed by Sitzmann et al. and Nakajima et al. for introducing CNT moieties in the coordination sphere of divalent barium and europium were demonstrated with other divalent lanthanides forming homoleptic [Ln^{II}(η^9-CNT)$_2$] compounds (Ln = Eu, Sm, Tm, Yb).[11] In this work, a key feature is that the CNT ligand in homoleptic sandwich compounds can be readily replaced by tetrahydrofuran or acetonitrile.[10a] In the case of trivalent dysprosium, a partial displacement has also been observed in the heteroleptic compound [(CNT)Dy^{III}(η^8-COT)].[10c] This observation is a rather unexpected finding in view of the classic chemistry of lanthanide-cyclopentadienyl derivatives, which generally coordinates to the lanthanide ion in almost all cases in an irreversible manner.[12] Inspired by the labile nature of the CNT ligand, we envisioned that this original property could also be observable in heteroleptic trivalent sandwich compounds of the type [(CNT)Ln^{III}(η^8-COT)], which were recently reported.[10b,c]

The concept is to de-coordinate the CNT ligand selectively and in a reversible manner via a solvation process. Upon this, the [Ln(η^8-COT)]$^+$ fragment should

[*] L. Münzfeld, M. Dahlen, A. Hauser, R. Köppe, P. W. Roesky
Institute of Inorganic Chemistry, Karlsruhe Institute of Technology (KIT)
Engesserstrasse 15, 76131 Karlsruhe (Germany)
E-mail: roesky@kit.edu

N. Mahieu, J. Moutet, M. Tricoire, G. Nocton
Laboratoire de Chimie Moléculaire (LCM), UMR 9168, CNRS, Ecole Polytechnique, Institut polytechnique Paris
Route de Saclay, 91120 Palaiseau (France)

L. La Droitte, O. Cador, B. Le Guennic
Univ Rennes, CNRS, ISCR (Institut des Sciences Chimiques de Rennes), UMR 6226
35000 Rennes (France)

E. Moreno-Pineda
Depto de Química-Física, Facultad de Ciencias Naturales, Exactas y Tecnología, Universidad de Panamá (Panamá)
E-mail: eufemio.moreno@up.ac.pa

E. Moreno-Pineda, M. Ruben
Institute of Nanotechnology (INT), Karlsruhe Institute of Technology (KIT)
Hermann-von-Helmholtz-Platz 1, 76344 Eggenstein-Leopoldshafen (Germany)
E-mail: mario.ruben@kit.edu

S. K. Kuppusamy, M. Ruben
Institute for Quantum Materials and Technologies (IQMT), Karlsruhe Institute of Technology (KIT)
Hermann-von-Helmholtz-Platz 1, 76344 Eggenstein-Leopoldshafen (Germany)

M. Ruben
Centre Européen de Science Quantique (CESQ), Institut de Science et d'Ingénierie Supramoléculaires (ISIS), UMR 7006, CNRS, Université de Strasbourg
8 allée Gaspard Monge, BP 70028, 67083 Strasbourg Cedex (France)

remain intact due to the strong bonding of the dianionic COT-ligand to the trivalent lanthanide ion. Removing of the CNT ligand would induce severe changes to the Ln ion's coordination sphere, respectively ligand field, and consequently significantly alter its electronic structure, possibly resulting in observable changes of physical properties.

Results and Discussion

Upon addition of THF to solid samples of these [(CNT)Ln(η^8-COT)] (Ln = La, Ce, Nd, Tb, Er) complexes, an immediate colour change of the insoluble materials can be observed (La: orange to colourless; Ce: green to light-yellow (at −10 °C) or green to red (at room temperature, see below); Nd: yellow to green; Tb: orange to colourless; Er: orange to light-pink). A colour change is often indicative for the transformation of the chemical environment of lanthanide ions; in the present scenario, the colour change is very likely due to THF coordination.[10a,c]

Structural Characterisation

All [Ln(thf)$_x$(η^8-COT)][CNT] compounds are slightly soluble in hot THF and readily form suitable crystals for X-Ray diffraction upon cooling saturated hot solutions (see Supporting Information section 2.3 for details). According to X-Ray diffraction analysis, the obtained complexes were classified in three categories (Scheme 1): Category **I** consists of [(η^4-CNT)La(thf)$_2$(η^8-COT)] (**1**) and [(η^4-CNT)Ce(thf)$_2$-(η^8-COT)] (**2$_{rt}$**, rt = crystallisation at room temperature). These compounds feature a slipped η^4-coordination of the CNT ring and do not form ionic species. Category **II** comprises of three ionic [Ln(thf)$_4$(η^8-COT)][CNT] (Ln = Ce-**2$_{lt}$**, Nd-**3**, Tb-**4**; lt = low temperature, crystallisation at −10 °C) species, in which the CNT-ring is entirely decoordinated. Category **III** only consists of the ionic species [Er(thf)$_3$(η^8-COT)][CNT] (**5**), with a lower THF coordination number of three. Hence, different coordination modes develop along the lanthanide series and can be explained by the decreasing ionic radii. Interestingly, Ce is the transition point between the slipped sandwich structures, found in category **I**, and the ionic species of categories **II** and **III**, as it can be present in both motifs depending on the crystallisation conditions. Hence, the slipped ligand structure of category **I** can be interpreted as an intermediate en route to complete CNT ligand substitution. It is important to note that the formation of compounds **1**–**5** is entirely reversible, e.g., drying these compounds under reduced pressure results in the corresponding precursors [(CNT)Ln(η^8-COT)], similarly as observed for the [Ln(η^9-CNT)$_2$] complexes.[10a] Note that a related outcome was shown with other types of coordinating ligands.[10a,13] The [(η^4-CNT)La(CH$_3$CN)$_2$(η^8-COT)] (**1$_{MeCN}$**) crystal structure is depicted in Figure S17.

Compounds **1** and **2$_{rt}$** (category **I**) feature double fold THF coordination to the central trivalent Ln ion and a heavily bent η^4-CNT ligand (Figure 1). The Ln-C$_{CNT}$ distances range from 2.901(3)–3.131(2) Å (La)/2.870(2)–3.142(2) Å (Ce) for the four close carbon atoms to up to 3.711(3)–4.595(3) Å (La)/3.619(2)–4.632(2) Å (Ce) for the opposing ones. The bending angle of the CNT-ring accounts for 23.5° (La)/21.9° (Ce) (Figures S11 and S12), underpinning the η^4-coordination mode. Due to the large ionic radii of La^{III} and Ce^{III}, THF can coordinate to the metal atom without replacing the CNT-ligand entirely. With values of 2.0287(4) Å (La)/1.9940(4) Å (Ce) for the Ln-Ct$_{COT}$ (Ct = ring centroid) and 2.648(2) Å as well as 2.619(2) Å (La)/2.5960(13) Å and 2.6340(12) Å (Ce) for the respective Ln-O$_{THF}$ distances, both are in the expected range.[14]

The retention of an uncharged structural motif also rationalises the low recoverable yields of 65 % (**1**-La) and 71 % (**2$_{rt}$**-Ce) from solvation experiments, due to tentatively higher solubility in THF. Interestingly, the La species **1** exhibits the neutral motif regardless of the crystallisation conditions. In contrast, the Ce solid-state structure depends on the crystallisation temperature. Crystallisation at room temperature results in the selective formation of red crystals of **2$_{rt}$**. In contrast, quick cooling to −10 °C without storage at room temperature solely gives light-yellow crystals of **2$_{lt}$** in 90 % yield (see category **II**). Once formed, **2$_{lt}$** is stable at room temperature in a THF containing atmosphere.

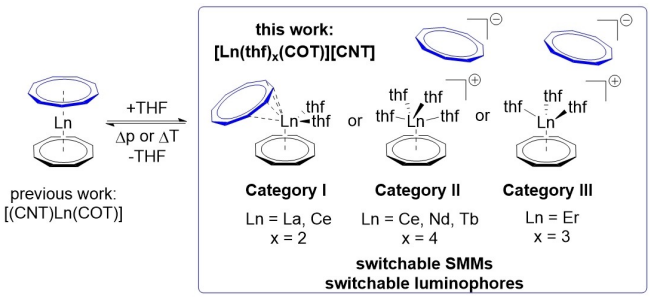

Scheme 1. Schematic depiction of the reversible solvation process in [(CNT)Ln(COT)]/[Ln(thf)$_x$(COT)][CNT] (x = 2–4) systems. The THF solvated complexes are obtained by adding the solvent to the solid precursor—[(CNT)Ln(COT)]—complexes. Application of dynamic vacuum resulted in the removal of the coordinated THF solvents, thereby forming the precursor complexes. The solvation and desolvation processes are reversible, as inferred from the Raman spectroscopic studies (vide infra). Δp and ΔT indicate pressure or temperature gradients, respectively.

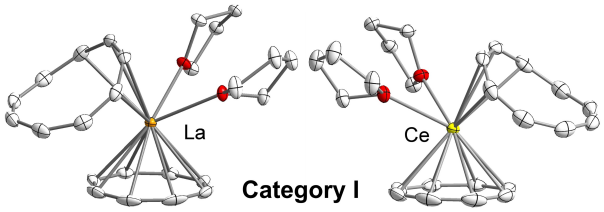

Figure 1. Molecular structures of [(η^4-CNT)La(thf)$_2$(η^8-COT)] (**1**, left) and [(η^4-CNT)Ce(thf)$_2$(η^8-COT)] (**2$_{rt}$**, right) in the solid state. Hydrogen atoms are omitted for clarity. Thermal ellipsoids are depicted at 50 % probability. C: colourless; O: red; La: orange; Ce: yellow.[15]

Category **II** comprises the three [Ln(thf)$_4$(η^8-COT)][CNT] (Ln = Ce-**2$_{lt}$**, Nd-**3**, Tb-**4**) compounds based on large to medium sized lanthanide ions. The molecular structures of complexes **2$_{lt}$**, **3** and **4** in the solid state exhibit a symmetry generated disordered COT moiety, however only one part of the disordered structure is discussed here (see Supporting Information for further details).

All three complexes have four molecules of THF coordinated to the central lanthanide ion, completely replacing the formerly η^9-coordinated CNT-ligand, while leaving the [Ln(η^8-COT)]$^+$ fragment intact (Figure 2). Two of the THF ligands are almost perpendicular to the COT-ring plane, while the others are rotated out of plane by approximately 90°. The Ln-Ct$_{COT}$ distances decrease from 2.005(3) Å (**2**) over 1.960(3) Å (**3**) to 1.887(2) Å (**4**), reflecting the decreasing ionic radii along the series. Likewise, the Ln–O distances average at decreasing values of 2.541 Å (**2$_{lt}$**), 2.512 Å (**3**) and 2.454 Å (**4**).

With [Er(thf)$_3$(η^8-COT)][CNT] (**5**) category **III** consists of only one compound. The molecular structure of **5** in the solid state shows symmetry generated disordered COT-, CNT- and THF-moieties; only one part of the disordered structure will be discussed here (see Supporting Information for further details). As observed within category **II**, complex **5** exhibits an ionic motif with THF ligands replacing the initially bound CNT-ring.

However, the smaller ionic radius of erbium lowers the number of coordinated THF molecules from four to three (Figure 3). Despite this change in coordination number, the Er–Ct$_{COT}$ distance of 1.726(3) Å smoothly continues above-described trend for decreasing Ln–Ct$_{COT}$ distances with decreasing ionic radii. The same applies for the Er–O distances, which average at 2.303 Å. Remarkably, the Er–Ct$_{CNT}$ distance of 5.4071(4) Å is significantly shorter than the Ln–Ct$_{CNT}$ distances found for **2**, **3** and **4**. As the smaller ionic radius of Er^{III} alone does not justify such a significant difference, we assume packing effects in the solid state to play a crucial role.

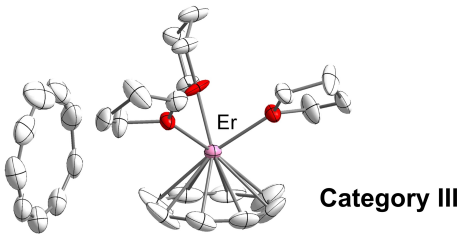

Figure 3. Molecular structure of [Er(thf)$_3$(η^8-COT)][CNT] **5** in the solid state. Hydrogen atoms as well as one part of the disordered COT-, CNT- and THF- moieties are omitted for clarity. Thermal ellipsoids are depicted at 50% probability. C: colourless; O: red; Er: purple.[15]

Raman Spectroscopic Investigations Towards the Reversibility

To trace the process in the solid-state, detailed Raman spectroscopic investigations were performed. The Raman spectra of vacuum dried crystalline samples of **1**–**5**, match those of the corresponding solvate free [(CNT)Ln(η^8-COT)] compounds, indicating that a negative pressure gradient can act as external stimulus for the complete removal of THF (Figures S3–S7). This of course involves the removal of THF by the attached vacuum pump, making the process irreversible in itself as THF has to be manually added for the resolvation to take place. Towards an entirely reversible and self-sufficient process, investigations in a closed glass compartment were performed trying to use a temperature gradient as stimulus. De-coordination of THF was triggered by the heating effect of a laser. After switching off the laser, the THF again coordinates to the metal replacing the CNT ligand (see Video S2).

The sample compartment contained deuterated THF (THF-d_8) as solvation source and the compound **2$_{lt}$** as an example for the [Ln(thf)$_x$(η^8-COT)][CNT] series (see Supporting Information page 8 for detailed preparation methods). THF-d_8 can readily be detected by Raman spectroscopy due to intense bands between 2000 cm^{-1} and 2300 cm^{-1} arising from C–D vibrations. These C–D bands are distinctly separated from the C–H bands of [(η^9-CNT)Ce(η^8-COT)], making them an ideal target for probing the THF-d_8 content. Without a sufficient external stimulus these bands are very dominant in the spectrum (Figure 4, blue spectrum). Additionally, the characteristic band of the Ln-CNT-ring vibration mode at 140 cm^{-1} cannot be observed, indicating that the CNT ligand is not present in the inner coordination sphere. Aside from spectroscopic evidence, the solvated species **2$_{lt}$** can easily be identified by its colour (**2$_{lt}$**: light yellow, **2$_{rt}$**: red, [(η^9-CNT)Ce(η^8-COT)]: green) and its intense photoluminescence when irradiated

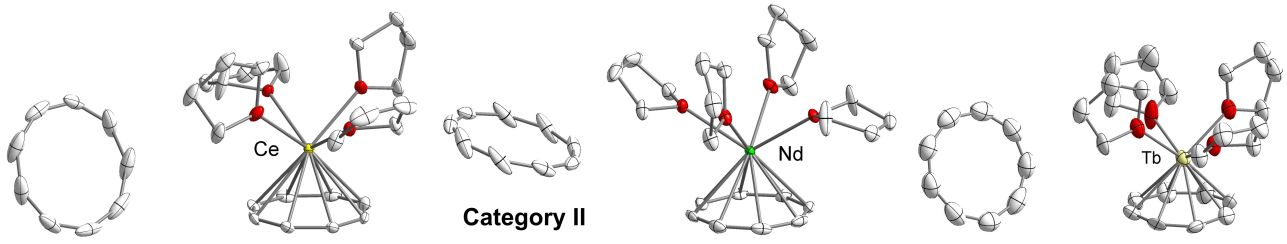

Figure 2. Molecular structures of [Ln(thf)$_4$(η^8-COT)][CNT] (Ln = Ce (**2$_{lt}$**) left, Nd (**3**) middle, Tb (**4**) right) in the solid state. Hydrogen atoms as well as one part of the disordered η^8-COT-ligand are omitted for clarity. Thermal ellipsoids are depicted at 50% probability. C: colourless; O: red; Ce: yellow; Nd: green; Tb: light yellow.[15]

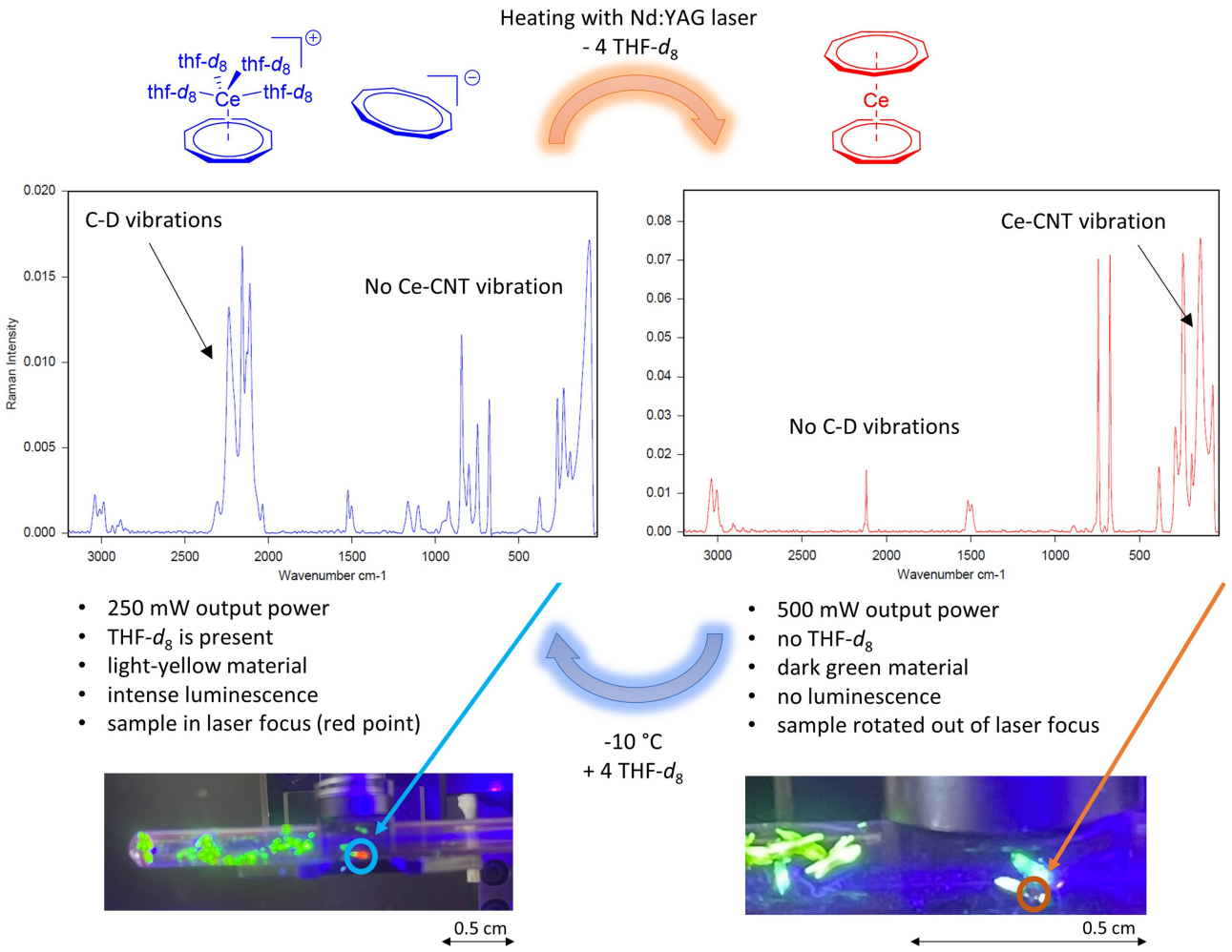

Figure 4. Conversion of $\mathbf{2_{lt}}$ to [(η^9-CNT)Ce(η^8-COT)] inside a Raman spectrometer. Top left: Stable Raman spectrum of $\mathbf{2_{lt}}$ recorded at 250 mW laser output power. Bottom left: luminescent crystals of $\mathbf{2_{lt}}$ and laser focus point (red marker in blue circle) after measurement at 250 mW. Top right: Raman spectrum recorded at 500 mW, clearly indicating the loss of THF-d_8 and presence of [(η^9-CNT)Ce(η^8-COT)]. Bottom right: enlarged picture of the irradiated crystal. The small area of approximately 0.2×0.2 mm (red circle) where the laser beam was focused exhibits a change in colour and does not luminesce anymore.

with UV-light (see below, no UV response for $\mathbf{2_{rt}}$ and [(η^9-CNT)Ce(η^8-COT)]).

As mentioned above, the desolvation / solvation process can be realised within a Raman spectrometer equipped with a Nd:YAG laser ($\lambda = 1064$ nm). We found that the laser can be used as efficient heating source at high input power. In fact, the laser beam allows to selectively remove THF from the sample material on a spatially confined area. While stable spectra of $\mathbf{2_{lt}}$ can be obtained over hours at medium input power (250 mW), an increase in input power (500 mW) leads to fast removal of THF, as indicated by single scan spectra (approximately 20–30 s transition time, see Video S1). Interestingly, the sample area first changes colour to red (presumably $\mathbf{2_{rt}}$) after five scans, before turning green ([(η^9-CNT)Ce(η^8-COT)]) after approximately 15 scans. This agrees with the suggestion of $\mathbf{2_{rt}}$ being an intermediate species in the examined systems. Continuous scan acquisitions doubtlessly show that all resonances stemming from THF-d_8 vanish, yielding a Raman spectrum that is equivalent to isolated crystalline [(η^9-CNT)Ce(η^8-COT)] (Figure 4, red spectrum). Optical inspection of the sample surface strongly suggests that the laser beam is capable of desolvating compound $\mathbf{2_{lt}}$ in a spatially resolved manner (Figure 4, bottom right). As described above, this process can be reverted by cooling the sample material. After having established the reversible transformation between [(CNT)Ln(η^8-COT)] and **1**–**5**, we moved towards elucidating the photoluminescence and the magnetic behaviour of selected compounds.

Photoluminescence

In the cases of Ce and Tb, significant differences were observed between the photoluminescence (PL) properties of the solvent-free [(η^9-CNT)Ln(η^8-COT)] (Ln = Ce, Tb) sandwich complexes and the solvated species $\mathbf{2_{lt}}$ and **4**. While the former ones do not show any remarkable light emission, $\mathbf{2_{lt}}$

and **4** show intense photoluminescence upon excitation with UV-light.

[(η^9-CNT)Ce(η^8-COT)] is a green solid, which immediately turns light-yellow upon addition of THF at −10 °C, forming compound $\mathbf{2_{lt}}$. The solvated species $\mathbf{2_{lt}}$ shows intense photoluminescence upon excitation with UV-light (note: THF addition at room temperature initially gives $\mathbf{2_{rt}}$, as red material, which does not show luminescence response). When dried, the colour of the solid material changes back from yellow to green within seconds, indicating the renewed formation of [(η^9-CNT)Ce(η^8-COT)].

For [(η^9-CNT)Ce(η^8-COT)] no luminescence is detectable (red line in Figure 5, Video S3). The photoluminescence (PL) spectra of $\mathbf{2_{lt}}$ express two broad characteristic approximately gaussian shaped bands at about 500 nm and 540 nm at 298 K (dashed dark blue line in Figure 5),[16] which both structure upon cooling to 77 K (blue line in Figure 5). Note that our experimental setup does not allow quantitative comparison, the spectra in Figure 5 are therefore normalised. The emissive bands may be assigned to transitions from the lowest-excited $5d^1$ (^2D) level to the $^2F_{5/2}$ (λ_{max} = 505 nm) and $^2F_{7/2}$ (λ_{max} = 540 nm) spin-orbit levels of the $4f^1$ configuration.[16,17] While the lower energy emission

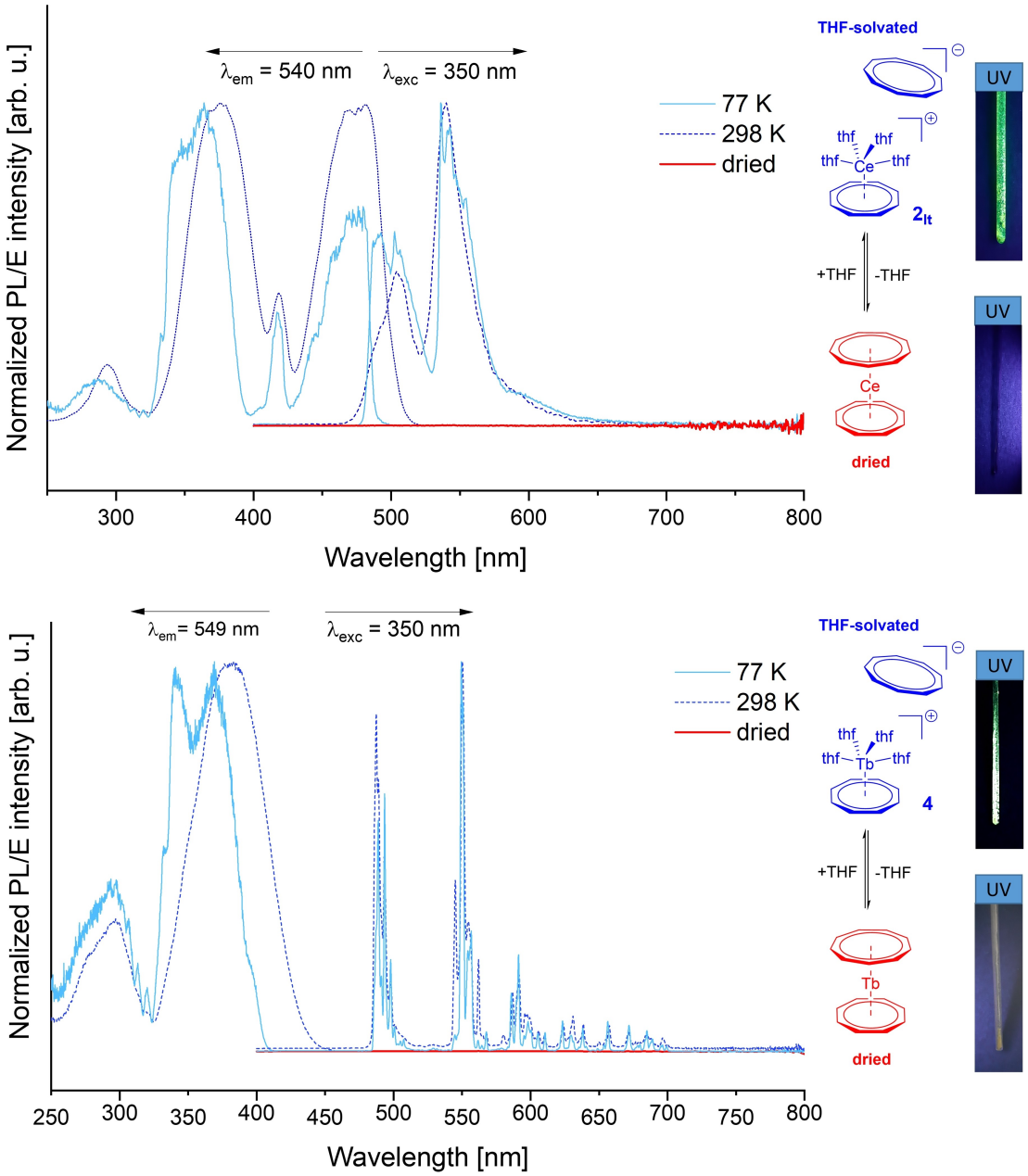

Figure 5. Excitation and emission spectra of $\mathbf{2_{lt}}$ [(Ce)(thf)$_4$(η^8-COT)][CNT] (top) and **4** [(Tb)(thf)$_4$(η^8-COT)][CNT] (bottom). PL and PLE spectra were excited (λ_{exc})/recorded (λ_{em}) at the depicted wavelengths and temperatures (Blue line: $\mathbf{2_{lt}/4}$ at 77 K. Dark blue dashed line: $\mathbf{2_{lt}/4}$ at 298 K. Red line: $\mathbf{2_{lt}/4}$ after drying in vacuo for 60 s at 298 K).

band does not shift upon a temperature increase, the higher energy band shows a slight redshift leading to slightly different energy separations of 1868 cm^{-1} (77 K) and 1254 cm^{-1} (298 K). Such behaviour was observed before by e.g., Edelmann and Wickleder et al.[17] Besides a small redshift in the onset upon increasing the temperature, the photoluminescence excitation (PLE) spectra look alike at both temperatures with maxima at approximately 350–375 nm and 475 nm. Lifetimes were found to vary from $\tau \approx 60$ ns to 90 ns (no significant temperature dependence, Table S13) and are in the expected range for the parity allowed 4f–5d transition.[16] In $\mathbf{2_{lt}}$, the CNT-ligand is replaced by four THF molecules, resulting in a similar ligand field configuration as described for $[Ce(COT)I(thf)_3]$.[14c] As the energy states of the excited ^2D level are known to vary as a function of the ligand sphere, PL spectroscopy of $[Ce(COT)I(thf)_3]$ should express slightly different transition energies than $\mathbf{2_{lt}}$ but otherwise resemble the latter.[16b] As expected, the relation is nicely reflected in very similar luminescence spectra for both compounds (Figure S18).

Analogous to the $[(\eta^9\text{-CNT})Ce(\eta^8\text{-COT})]/\mathbf{2_{lt}}$ system, $[(\eta^9\text{-CNT})Tb(\eta^8\text{-COT})]$ changes colour from yellow to colourless when laced with THF giving the solvent-coordinated compound **4**. Complex **4** emits green luminescence when excited with UV light. Upon drying in vacuo, the change in colour is reversed and the observed luminescence ceases (red line in Figure 5 bottom, Video S4). Again, this is strongly indicative of the formation of $[(\eta^9\text{-CNT})Tb(\eta^8\text{-COT})]$ and in agreement with the Raman spectroscopic analysis. Obtained emission spectra for **4** are consistent with reported Tb^{III} spectra in literature showing lanthanide centred emission based on an energy transfer from the ligand to the excited $^5D_4$ terbium level followed by emissive $^5D_4 \rightarrow {}^7F_n$ phosphorescence transitions.[18] Upon temperature variation there was no significant change in energy regarding the emission spectra. However, for PLE, a loss in structure and a red-shift in the onset was observed when switching to room temperature. Lifetimes of the excited states of **4** were determined to be $\approx$95 µs at room temperature and $\approx$570 µs at 77 K (Table S15), being in the range of literature values.[18] Although PLE spectra differ in energetic position and band shape, which is assigned to the different ligands, emission spectra of **4** and $[Tb(COT)I(thf)_2]$[10c] look very alike, confirming the emission taking place from the lanthanide centre regardless of the differences in the coordination environment (see Figure S19).

Magnetic Properties

The manipulable properties upon (de)solvation of the complexes have been undoubtedly demonstrated through Raman and PL spectroscopic studies. Moreover, the change in colour, along with the PL characteristics, clearly indicate a change in the electronic configuration of the systems. To test whether the reversible solvation process influences further the magnetic properties, we investigated the SMM behaviour of these systems. Complexes **5** and $[(\eta^9\text{-CNT})Nd(\eta^8\text{-COT})]$ were found to behave as SMMs, hence in the following we will describe the magnetic data of these two complexes. The objective of the following section is to emphasise the discrimination of magnetic properties between the solvated and desolvated complexes within the Er and Nd systems. The complex $[(CNT)Er(\eta^8\text{-COT})]$ has been shown to be an SMM,[10b] exhibiting an $U_{eff} = 361(1)$ K (at zero field) and $U_{eff} = 376(1)$ K (under an optimal field of 2 kOe), resulting in the observation of open hysteresis loops until temperatures as high as 10 K. In contrast, complex **5** shows distinctly different dynamic characteristics as follows (Figures 6, S20): (*i*) the frequency-dependent out-of-phase magnetic susceptibility ($\chi''_M(\upsilon)$) at zero field ranges from 2 K to 8.4 K (*cf.* $[(CNT)Er(\eta^8\text{-COT})]$ with $\chi''_M(\upsilon)$ ranging from 2 K to 26 K); (*ii*) at 2 K the maximum in $\chi''_M(\upsilon)$ is centred at 233 Hz (*cf.* in $[(CNT)Er(\eta^8\text{-COT})]$ the maximum lies below 1 Hz at 2 K); (*iii*) in contrast, analysis of the relaxation times of **5** at zero field shows that the relaxation occurs through a multi-step process, where the Raman relaxation plays an important role, leading to a smaller barrier, $U_{eff} = 96.7(1)$ K (*cf.* $U_{eff} = 361(1)$ K in $[(CNT)Er(\eta^8\text{-COT})]$)—the *n* parameter being much smaller than expected for Kramers ions, denoting active acoustic and optic phonons[19] (*iv*) no open hysteresis loops were found for the THF coordinated complex **5**, while open loops as high as 10 K were found for $[(CNT)Er(\eta^8\text{-COT})]$. Similar to $[(CNT)Er(\eta^8\text{-COT})]$, application of an optimal field of 2 kOe (Figure S21) slightly decreases relaxation rate, yielding an $U_{eff} = 118.9(1)$ K (Figure S22 and S23). Note that although both Er-COT complexes are dominated by ligand-metal pair anisotropy,[20] the relaxation dynamics upon removal of CNT ligand and addition of THF molecules are considerably different. This observation implies that the CNT ligand exerts a relatively large equatorial anisotropy, which further enhances the Er-COT dynamics. Note that for $[(CNT)Er(\eta^8\text{-COT})]$ a saturation value at 2 K and 7 T of $\approx 5\ \mu_\beta$ is found, characteristic of an $m_J = |\pm 15/2>$ ground doublet of the $^4I_{15/2}$ multiplet.[3h,21] In contrast, for **5** a saturation value of 4.6 μ_β is obtained at the same field and temperature (Figure S27), indicating a mixture of m_J states which can induce faster relaxation (*vide infra*).

The results previously observed for $[(CNT)Er(\eta^8\text{-COT})]$ and the here reported THF coordinated counterpart **5** clearly show that upon solvation, respectively desolvation, the SMM character of the system can be modulated. This facilitates clear discrimination between slow and fast relaxation of the magnetisation. However, the SMM character cannot be shut off entirely.

In contrast to **5** and $[(CNT)Er(\eta^8\text{-COT})]$, an even more distinct behaviour was found for $[(\eta^9\text{-CNT})Nd(\eta^8\text{-COT})]$ and the THF coordinated complex **3**. No SMM signature was found for **3** at zero field or upon application of DC fields. Remarkably, $[(\eta^9\text{-CNT})Nd(\eta^8\text{-COT})]$ is an SMM upon application of an optimal field of $H_{DC} = 2$ kOe (Figure S24). A clear frequency-dependent behaviour is observed in the ac susceptibility studies. The $\chi''_M(T)$ shows a maximum centred at ca. 8 K (at the highest frequency), which shifts towards lower temperatures for lower frequencies (Figure S25). The $\chi''_M(\upsilon)$ similarly reveals a maximum centred at 13 Hz at 2 K, which swiftly shifts towards higher

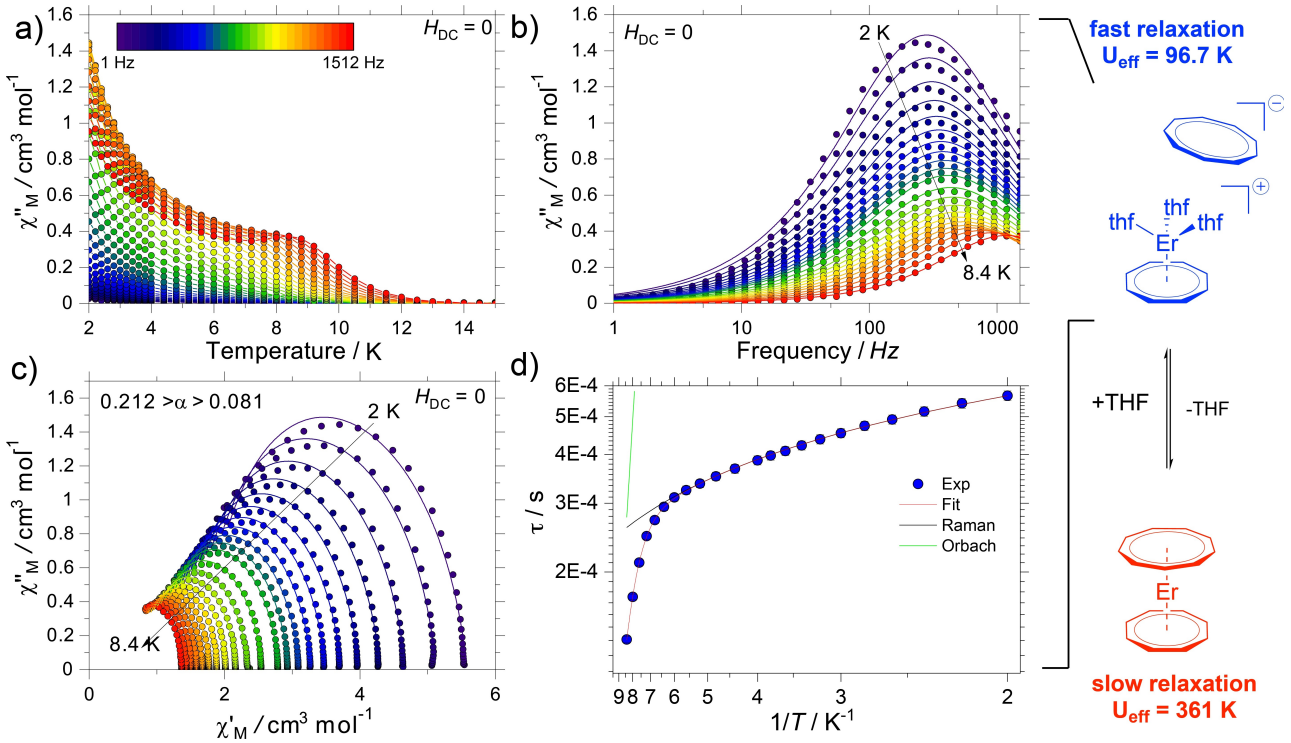

Figure 6. Dynamic magnetic data for the THF solvated complex **5** at zero field with an oscillating AC field of 3.5 Oe. a) $\chi''_M(T)$ and b) $\chi''_M(\upsilon)$ plots show the less efficient SMM properties compared to the unsolvated analogue [(η^9-CNT)Er(η^8-COT)]. Solid lines in panel (b) are fit to the generalised Debye model. c) Cole-Cole plots and distribution of relaxation times. d) Relaxation analysis for the obtained τ. The relaxation data at zero field were fitted to $\tau^{-1} = \tau_0^{-1}\exp(-\frac{U_{eff}}{kT}) + CT^n$, with the best fit resulting in U_{eff}=96.7(1) K, τ_0=2.54(4)×10^{-9} s^{-1}, C=1214(6) s^{-1}K^{-n}, n=0.541(3).

frequencies upon increasing the temperature (Figure 7). Note that solely Raman process is responsible for the τ(T) profile, as commonly observed in other Nd-based SMMs.[22] Upon application of DC fields, the Direct process also becomes active, as revealed by the simulation of the τ(H) data (Figure S24c). Note that $\chi'_M(\upsilon)$ and the χ_S/χ_T ratio for both **5** and [(η^9-CNT)Nd(η^8-COT)] show that just a fraction of the samples relaxes (Tables S17–S19 and Figure S20c, S22a, S25a). This fractional relaxation might be associated to structural distortions in [(η^9-CNT)Nd(η^8-COT)]. For **5**, a deviation from the three legged piano stool motif, that was established by SCXRD, might account for the differences.[10c,23] Nevertheless, the switchable character of these systems remains intact.

Theoretical Calculations

CASSCF/RASSI-SO calculations were performed on the XRD crystal structures of **5**, [(CNT)Er(η^8-COT)], **3** and [(η^9-CNT)Nd(η^8-COT)] to give more insight into their magnetic properties (See Supporting Information for computational details). Computed energy levels, composition of the g-tensor and the main components of the wavefunction for each m_J state of the corresponding ground-state multiplet are given in Tables S20–S23. On this basis, a good agreement is observed with the experimental thermal variation of $\chi_M T$ and magnetisation versus field data at 2 K for [(η^9-CNT)Nd(η^8-COT)] and **5**, as presented in Figures S26 and S27. Calculations show that the SMM properties observed in [(CNT)Er(η^8-COT)] arise from the Ising-type anisotropy of the ground state (Figure 8) and the highly pure character of the m_J states, comprising the ground and first excited state as well as the large energy splitting between these (Table S20). In contrast, CASSCF calculations of the THF adduct **5** reveal that, although the m_J composition of the ground doublet is highly pure (Table S21), the first excited m_J state is rather mixed and lower in energy than in [(CNT)Er(η^8-COT)], potentially allowing the system to reverse magnetisation faster than in [(CNT)Er(η^8-COT)].[10b] This difference of relaxation pathway between [(CNT)Er(η^8-COT)] and the solvated complex **5** is further visible with the computed magnetic transition moments, presented in Figure S28 which also reveals a low contribution of the quantum tunnelling of magnetisation (QTM) mechanism up to the second excited state for [(CNT)Er(η^8-COT)].

While for **5**, transverse transition matrix elements indicate a relaxation of the magnetisation through the ground state and the first excited state with faster thermally assisted QTM.

Similarly, computations rationalise the absence of SMM behaviour for the THF coordinated complex **3** by unveiling a pseudo-planar anisotropy of its ground doublet state, visible in Figure 8, with g-values of g_z=3.1, g_x=0.8 and g_y=

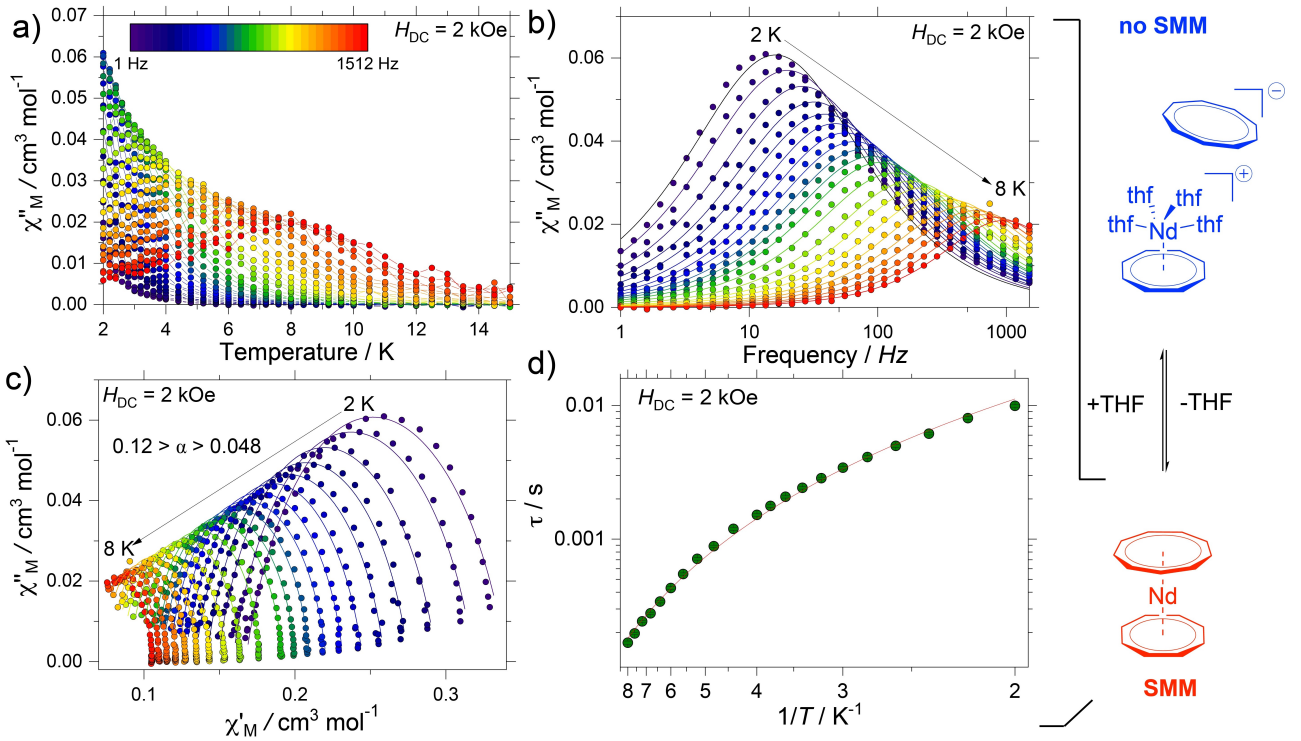

Figure 7. Dynamic magnetic data for [(η^9-CNT)Nd(η^8-COT)] with H_{DC} = 2 kOe employing an oscillating AC field of 3.5 Oe. a) $\chi''_M(T)$ and b) $\chi''_M(\upsilon)$ show the SMM properties. c) Cole-Cole plots and distribution of relaxation times. Solid lines in panel (b) and (c) are fit to the Debye model. d) Analysis for the obtained $\tau(T)$ dependence shows that the relaxation occurs mainly though a Raman process. The dotted line corresponds to the fitting to a model based solely on the Raman process, i.e., $\tau^{-1} = CT^n$ with C = 9.98(2) s^{-1} K^{-n} and n = 3.06(4).

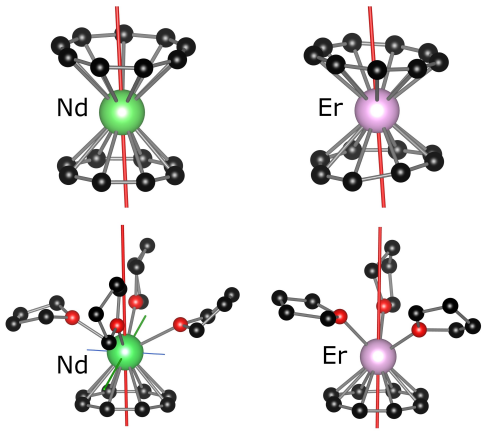

Figure 8. Orientation of the g-tensor components g_z (red axis), g_y (green axis) and g_x (blue axis) represented with relative size based on their respective g-value (Tables S20–S23) for [(η^9-CNT)Nd(η^8-COT)] (top left), [(CNT)Er(η^8-COT)] (top right), **3** (bottom left) and **5** (bottom right), obtained from CASSCF calculations.

2.0, and highly mixed $m_J = |\pm 7/2>$ (46.8 %) + $|\pm 5/2>$ (30.3 %) (Table S22). Likewise, to [(CNT)Er(η^8-COT)], the SMM behaviour of [(η^9-CNT)Nd(η^8-COT)] upon application of an external field arises from its almost pure $m_J = |\pm 5/2>$ (95.0 %) ground doublet state (Table S23).

Additionally, a slow relaxation of the magnetisation seems possible via its first excited state despite the small QTM contribution in the ground state, much less pronounced than in **3** (Figure S28). Calculations were also performed on the XRD crystal structure of $\mathbf{2_{lt}}$, [(η^9-CNT)Ce(η^8-COT)], **4** and [(η^9-CNT)Tb(η^8-COT)] to interpret the absence of slow relaxation of the magnetisation in these compounds (Tables S24–S27). For $\mathbf{2_{lt}}$ and [(η^9-CNT)Ce(η^8-COT)], the ground state was found pure $m_J = |\pm 1/2>$ (Tables S24 and S25), explaining the planar anisotropy, and thus discarding the possibility of SMM behaviour. For **4** and [(η^9-CNT)Tb(η^8-COT)], the computations show a non Ising-type anisotropy of the non-degenerated ground state with a pure $m_J = |0>$ (Tables S26 and S27), leading again to the impossibility of SMM behaviour. The calculations provide an explanation for the different magnetic behaviours between solvated and desolvated compounds through the computed energy levels and wavefunctions, specifically for the absence of SMM behaviour for **3**, while [(η^9-CNT)Nd(η^8-COT)] is a modest SMM upon application of an external field.

Conclusion

Our findings demonstrate that the properties of different [(CNT)Ln(η^8-COT)]/[Ln(thf)$_x$(η^8-COT)][CNT] systems can be manipulated by reversible solvation or desolvation, respectively. These systems can be employed to orchestrate the SMM behaviour of the Nd and Er species as well as the

luminescence of the Ce and Tb complexes. This behaviour is facilitated by the labile nature of the CNT-ligand in the common organic donor solvent tetrahydrofuran. The process is repeatable and can be controlled by external pressure or temperature stimuli, enabling selective modification of the ligand sphere in a solid-to-solid transformation. An external heating approach using a Nd:YAG laser additionally allows to perform this process spatially resolved and self-sufficient in an inert vessel. The luminescent systems Ce and Tb are therefore capable of reaching a switch-like state at operating conditions. At the same time, the current chemical identity of the system can be monitored by Raman spectroscopy. Aided by optically guided devices as for example Raman microscopes, these results might give impulses towards the technical realisation of switchable SMMs and luminophores that can be targeted, controlled, and monitored in a spatially resolved manner. An important milestone towards high-performance switchable materials.

Acknowledgements

KIT is acknowledged for financial support. M.D. thanks the Fonds der Chemischen Industrie for the generous fellowship (No. 103581). A.H., M.R., and P.R. gratefully acknowledge financial support from the Deutsche Forschungsgemeinschaft (DFG, German Research Foundation) through the Collaborative Research Centre "4f for Future" (CRC 1573, project number 471424360) projects C1 and B2. E.M.-P. thanks the Panamanian National System of Investigators (SNI, SENACYT) and SENACYT (project PFID-FID-2021-60) for support. Parts of this work have received funding from the ERC under grant agreement No 716314 and from an ANR (French National Research Agency) granted collaborative project (ANR-19-CE07-0019-1). CNRS and Ecole polytechnique are thanked for financial support. N.M. thanks ENS Paris-Saclay. B.L.G. and L.L.D. thank the French GENCI/IDRIS-CINES centres for high-performance computing resources. Open Access funding enabled and organized by Projekt DEAL.

Conflict of Interest

The authors declare no competing interests.

Data Availability Statement

The data that support the findings of this study are available in the Supporting Information of this article.

Keywords: Lanthanides · Magnetism · Molecular Switches · Photoluminescence · Sandwich Compounds

[1] a) D. Gatteschi, R. Sessoli, J. Villain, *Single-Molecule Magnets*, Oxford University Press, Oxford, **2006**; b) J.-C. G. Bünzli, *Coord. Chem. Rev.* **2015**, *293–294*, 19; c) D. A. Gálico, A. A. Kitos, J. S. Ovens, F. A. Sigoli, M. Murugesu, *Angew. Chem. Int. Ed.* **2021**, *60*, 6130; *Angew. Chem.* **2021**, *133*, 6195.

[2] a) M. N. Leuenberger, D. Loss, *Nature* **2001**, *410*, 789; b) A. Ardavan, O. Rival, J. J. L. Morton, S. J. Blundell, A. M. Tyryshkin, G. A. Timco, R. E. P. Winpenny, *Phys. Rev. Lett.* **2007**, *98*, 057201; c) M. Mannini, F. Pineider, C. Danieli, F. Totti, L. Sorace, P. Sainctavit, M. A. Arrio, E. Otero, L. Joly, J. C. Cezar, A. Cornia, R. Sessoli, *Nature* **2010**, *468*, 417; d) M. Mannini, F. Pineider, P. Sainctavit, C. Danieli, E. Otero, C. Sciancalepore, A. M. Talarico, M.-A. Arrio, A. Cornia, D. Gatteschi, R. Sessoli, *Nat. Mater.* **2009**, *8*, 194; e) M. Urdampilleta, N.-V. Nguyen, J.-P. Cleuziou, S. Klyatskaya, M. Ruben, W. Wernsdorfer, *Int. J. Mol. Sci.* **2011**, *12*, 6656; f) S. Thiele, F. Balestro, R. Ballou, S. Klyatskaya, M. Ruben, W. Wernsdorfer, *Science* **2014**, *344*, 1135; g) C. Godfrin, A. Ferhat, R. Ballou, S. Klyatskaya, M. Ruben, W. Wernsdorfer, F. Balestro, *Phys. Rev. Lett.* **2017**, *119*, 187702; h) E. Moreno-Pineda, C. Godfrin, F. Balestro, W. Wernsdorfer, M. Ruben, *Chem. Soc. Rev.* **2018**, *47*, 501; i) M. Atzori, R. Sessoli, *J. Am. Chem. Soc.* **2019**, *141*, 11339; j) E. Coronado, *Nat. Rev. Mater.* **2020**, *5*, 87.

[3] a) C. A. P. Goodwin, F. Ortu, D. Reta, N. F. Chilton, D. P. Mills, *Nature* **2017**, *548*, 439; b) F.-S. Guo, B. M. Day, Y.-C. Chen, M.-L. Tong, A. Mansikkamäki, R. A. Layfield, *Angew. Chem. Int. Ed.* **2017**, *56*, 11445; *Angew. Chem.* **2017**, *129*, 11603; c) F.-S. Guo, B. M. Day, Y.-C. Chen, M.-L. Tong, A. Mansikkamäki, R. A. Layfield, *Science* **2018**, *362*, 1400; d) C. A. Gould, K. R. McClain, J. M. Yu, T. J. Groshens, F. Furche, B. G. Harvey, J. R. Long, *J. Am. Chem. Soc.* **2019**, *141*, 12967; e) J. P. Durrant, J. Tang, A. Mansikkamäki, R. A. Layfield, *Chem. Commun.* **2020**, *56*, 4708; f) R. K. McClain, C. A. Gould, K. Chakarawet, S. J. Teat, T. J. Groshens, J. R. Long, B. G. Harvey, *Chem. Sci.* **2018**, *9*, 8492; g) K. R. Meihaus, J. R. Long, *J. Am. Chem. Soc.* **2013**, *135*, 17952; h) L. Ungur, J. J. Le Roy, I. Korobkov, M. Murugesu, L. F. Chibotaru, *Angew. Chem. Int. Ed.* **2014**, *53*, 4413; *Angew. Chem.* **2014**, *126*, 4502.

[4] a) O. Sato, *Nat. Chem.* **2016**, *8*, 644; b) O. Cador, B. Le Guennic, F. Pointillart, *Inorg. Chem. Front.* **2019**, *6*, 3398.

[5] X.-D. Huang, G.-H. Wen, S.-S. Bao, J.-G. Jia, L.-M. Zheng, *Chem. Sci.* **2021**, *12*, 929.

[6] W.-B. Chen, Y.-C. Chen, J.-L. Liu, J.-H. Jia, L.-F. Wang, Q.-W. Li, M.-L. Tong, *Inorg. Chem.* **2017**, *56*, 8730.

[7] a) S. Fortier, J. J. Le Roy, C.-H. Chen, V. Vieru, M. Murugesu, L. F. Chibotaru, D. J. Mindiola, K. G. Caulton, *J. Am. Chem. Soc.* **2013**, *135*, 14670; b) D. E. Freedman, D. M. Jenkins, A. T. Iavarone, J. R. Long, *J. Am. Chem. Soc.* **2008**, *130*, 2884.

[8] a) X. Feng, C. Mathonière, I.-R. Jeon, M. Rouzières, A. Ozarowski, M. L. Aubrey, M. I. Gonzalez, R. Clérac, J. R. Long, *J. Am. Chem. Soc.* **2013**, *135*, 15880; b) C. Mathonière, H.-J. Lin, D. Siretanu, R. Clérac, J. M. Smith, *J. Am. Chem. Soc.* **2013**, *135*, 19083; c) M. Hojorat, H. Al Sabea, L. Norel, K. Bernot, T. Roisnel, F. Gendron, B. L. Guennic, E. Trzop, E. Collet, J. R. Long, S. Rigaut, *J. Am. Chem. Soc.* **2020**, *142*, 931.

[9] a) J.-L. Liu, Y.-C. Chen, Y.-Z. Zheng, W.-Q. Lin, L. Ungur, W. Wernsdorfer, L. F. Chibotaru, M.-L. Tong, *Chem. Sci.* **2013**, *4*, 3310; b) K. Suzuki, R. Sato, N. Mizuno, *Chem. Sci.* **2013**, *4*, 596.

[10] a) M. Xémard, S. Zimmer, M. Cordier, V. Goudy, L. Ricard, C. Clavaguéra, G. Nocton, *J. Am. Chem. Soc.* **2018**, *140*, 14433; b) L. Münzfeld, C. Schoo, S. Bestgen, E. Moreno-Pineda, R. Köppe, M. Ruben, P. W. Roesky, *Nat. Commun.* **2019**, *10*, 3135; c) M. Tricoire, L. Münzfeld, J. Moutet, N. Mahieu, L. La Droitte, E. Moreno-Pineda, F. Gendron, J. D. Hilgar, J. D. Rinehart, M. Ruben, O. Cador, B. Le Guennic, P. W. Roesky, G. Nocton, *Chem. Eur. J.* **2021**, *27*, 13558.

[11] a) M. D. Walter, G. Wolmershäuser, H. Sitzmann, *J. Am. Chem. Soc.* **2005**, *127*, 17494; b) K. Kawasaki, R. Sugiyama, T.

Tsuji, T. Iwasa, H. Tsunoyama, Y. Mizuhata, N. Tokitoh, A. Nakajima, *Chem. Commun.* **2017**, *53*, 6557.
[12] M. Dolg, H. Stoll, A. Savin, H. Preuss, *Theor. Chim. Acta* **1989**, *75*, 173.
[13] J. Moutet, J. Schleinitz, L. La Droitte, M. Tricoire, F. Pointillart, F. Gendron, T. Simler, C. Clavaguéra, B. Le Guennic, O. Cador, G. Nocton, *Angew. Chem. Int. Ed.* **2021**, *60*, 6042; *Angew. Chem.* **2021**, *133*, 6107.
[14] a) C. W. DeKock, S. R. Ely, T. E. Hopkins, M. A. Brault, *Inorg. Chem.* **1978**, *17*, 625; b) C. Meermann, K. Ohno, K. W. Törnroos, K. Mashima, R. Anwander, *Eur. J. Inorg. Chem.* **2009**, 76; c) K. Mashima, H. Takaya, *Tetrahedron Lett.* **1989**, *30*, 3697.
[15] Deposition Numbers 2125022 (for [(η^9-CNT)La(η^8-COT)]), 2125023 (for [(η^9-CNT)Ce(η^8-COT)]), 2125024 (for **1**), 2125025 (for $\mathbf{2_{rt}}$), 2125026 (for $\mathbf{2_{lt}}$), 2125027 (for **3**), 2125028 (for **4**), 2125029 (for **5**), and 2125030 (for **1** CH_3CN). contain the supplementary crystallographic data for this paper. These data are provided free of charge by the joint Cambridge Crystallographic Data Centre and Fachinformationszentrum Karlsruhe Access Structures service.
[16] a) K. W. Krämer, P. Dorenbos, H. U. Güdel, C. W. E. van Eijk, *J. Mater. Chem.* **2006**, *16*, 2773; b) P. N. Hazin, C. Lakshminarayan, L. S. Brinen, J. L. Knee, J. W. Bruno, W. E. Streib, K. Folting, *Inorg. Chem.* **1988**, *27*, 1393.
[17] M. Suta, N. Harmgarth, M. Kühling, P. Liebing, F. T. Edelmann, C. Wickleder, *Chem. Asian J.* **2018**, *13*, 1038.
[18] a) H. G. Brittain, J. H. Meadows, W. J. Evans, *Organometallics* **1983**, *2*, 1661; b) S. Shuvaev, O. Kotova, V. Utochnikova, A. Vaschenko, L. Puntus, V. Baulin, N. Kuzmina, A. Tzivadze, *Inorg. Chem. Commun.* **2012**, *20*, 73; c) Y. Chen, Z. Xing, S. Cao, Y. Wang, *J. Rare Earths* **2016**, *34*, 240.
[19] C. A. P. Goodwin, D. Reta, F. Ortu, N. F. Chilton, D. P. Mills, *J. Am. Chem. Soc.* **2017**, *139*, 18714.
[20] a) J. D. Rinehart, J. R. Long, *Chem. Sci.* **2011**, *2*, 2078; b) J. D. Hilgar, M. G. Bernbeck, J. D. Rinehart, *J. Am. Chem. Soc.* **2019**, *141*, 1913.
[21] a) Z. Zhou, J. McNeely, J. Greenough, Z. Wei, H. Han, M. Rouzières, A. Y. Rogachev, R. Clérac, M. A. Petrukhina, *Chem. Sci.* **2022**, *13*, 3864; b) S.-M. Chen, J. Xiong, Y.-Q. Zhang, Q. Yuan, B.-W. Wang, S. Gao, *Chem. Sci.* **2018**, *9*, 7540; c) J. J. Le Roy, I. Korobkov, M. Murugesu, *Chem. Commun.* **2014**, *50*, 1602.
[22] a) H. Wada, S. Ooka, T. Yamamura, T. Kajiwara, *Inorg. Chem.* **2017**, *56*, 147; b) J. Liu, D. Reta, J. A. Cleghorn, Y. X. Yeoh, F. Ortu, C. A. P. Goodwin, N. F. Chilton, D. P. Mills, *Chem. Eur. J.* **2019**, *25*, 7749; c) Y.-C. Chen, X.-S. Huang, J.-L. Liu, M.-L. Tong, *Inorg. Chem.* **2018**, *57*, 11782; d) M.-X. Xu, Y.-S. Meng, J. Xiong, B.-W. Wang, S.-D. Jiang, S. Gao, *Dalton Trans.* **2018**, *47*, 1966; e) H.-L. Zhang, X.-Y. Wu, J.-Z. Liao, X.-F. Kuang, W. Yang, C.-Z. Lu, *Dalton Trans.* **2018**, *47*, 1796; f) J. D. Rinehart, J. R. Long, *Dalton Trans.* **2012**, *41*, 13572; g) A. K. Jassal, N. Aliaga-Alcalde, M. Corbella, D. Aravena, E. Ruiz, G. Hundal, *Dalton Trans.* **2015**, *44*, 15774; h) S. K. Gupta, T. Rajeshkumar, G. Rajaraman, R. Murugavel, *Chem. Commun.* **2016**, *52*, 7168; i) K. S. Pedersen, A.-M. Ariciu, S. McAdams, H. Weihe, J. Bendix, F. Tuna, S. Piligkos, *J. Am. Chem. Soc.* **2016**, *138*, 5801; j) J. J. Baldoví, J. M. Clemente-Juan, E. Coronado, Y. Duan, A. Gaita-Ariño, C. Giménez-Saiz, *Inorg. Chem.* **2014**, *53*, 9976.
[23] a) A. K. Boudalis, M. Pissas, C. P. Raptopoulou, V. Psycharis, B. Abarca, R. Ballesteros, *Inorg. Chem.* **2008**, *47*, 10674; b) A. K. Boudalis, *Quantum Mater. Res* **2020**, *1*, e200004.

Manuscript received: December 8, 2022
Accepted manuscript online: January 18, 2023
Version of record online: February 14, 2023